Size Ratio Effects on Interparticle Interactions and Phase Behavior of Microsphere−Nanoparticle Mixtures

Angel T. Chan and Jennifer A. Lewis*

Materials Science and Engineering Department, Frederick Seitz Materials Research Laboratory, University of Illinois, Urbana−Champaign, Urbana, Illinois 61801

Received February 7, 2008. Revised Manuscript Received August 11, 2008

We investigate the interparticle interactions and phase behavior of microsphere−nanoparticle mixtures of high charge asymmetry and varying size ratio. In the absence of nanoparticles, negligibly charged microspheres flocculate as a result of van der Waals interactions. Upon addition of a lower critical nanoparticle volume fraction, the microspheres are stabilized by the formation of nanoparticle halos around each microsphere.[1,2] A weak attraction between the two species leads to a pronounced enhancement of the effective nanoparticle concentration near the microsphere surface relative to the bulk solution. Above an upper critical nanoparticle volume fraction, the microspheres undergo reentrant gelation. Binary mixtures, in which the effective nanoparticle size is reduced at a fixed microsphere diameter, exhibit a narrow window of stability that ultimately disappears with increasing ionic strength. By contrast, binary mixtures of varying microsphere diameter are stabilized at similar nanoparticle volume fractions and exhibit a broader window of stability with decreasing size ratio. This unexpected observation may arise from the reduced attraction between smaller microspheres because negligible differences in nanoparticle halo formation are observed in these mixtures.

Introduction

Colloidal suspensions are used in a wide range of applications, including inks,[3] ceramics,[4] pharmaceuticals,[5−7] and photonic crystals.[8−12] Such applications require exquisite control over colloidal stability and hence their interparticle interactions and phase behavior. Nanoparticle engineering offers a new paradigm by which suspension stability can be regulated. By investigating a model system composed of silica microsphere−polystyrene mixtures whose electrostatic interactions are carefully tuned, we recently demonstrated that important differences in system stability emerge depending on whether added nanoparticles serve as haloing, bridging, or depletant species.[1,2]

Nanoparticle haloing occurs when highly charged nanoparticles weakly segregate to regions near negligibly charged microsphere surfaces, thus mitigating the van der Waals attraction between microspheres that drives aggregation in their absence.[1,13] Recent theoretical[14] and simulation[15] efforts support the notion that nanoparticle halos form in such systems, leading first to colloidal stabilization above a lower critical nanoparticle volume fraction ($\phi_{nano}^{L,C}$) and, ultimately, to reaggregation at even higher nanoparticle volume fractions ($\phi_{nano}^{U,C}$) by a mechanism that differs qualitatively from the standard depletion attraction predicted by Asakura and Oosawa.[16] Nevertheless, the underlying mechanisms that foster nanoparticle haloing remain a subject of debate.

Karanikas and Louis[14] reported that nanoparticle halo formation is driven solely by an electrostatic repulsion between nanoparticles in solution; however, a significantly larger Debye screening length (i.e., higher effective nanoparticle volume fraction) is required to match our original experimental observations on silica microsphere−hydrous zirconia nanoparticle mixtures.[1,13] They found that the 2D packing fraction of nanoparticles around the microspheres is less than the close-packing limit at the onset of haloing-induced stabilization and that nanoparticle species undergo rapid diffusion between the halos and bulk solution under such conditions. Unlike strongly attractive mixtures in which the nanoparticle monolayers are static, they emphasize the dynamic nature of nanoparticle halos. They also explicitly modeled the effects of varying the nanoparticle hard-sphere (σ_{nano}) and effective ($\sigma_{nano}^{eff} = \sigma_{nano} + \lambda$, where λ is taken to be the Debye screening length) diameters at a fixed microsphere diameter on colloidal stability. They predicted that the window of stability, defined by $\phi_{nano}^{U,C}/\phi_{nano}^{L,C}$, increased with increasing effective nanoparticle diameter as well as microsphere−nanoparticle size ratio. They also predicted that the onset of colloidal stability occurs at lower nanoparticle volume fraction as the microsphere−nanoparticle size ratio increases.

Liu and Luijten[15] carried out computer simulations on binary mixtures of high size and charge asymmetry and found that a weak attraction (ca. several kT in magnitude) between microsphere−nanoparticle species is necessary to induce halo formation at the low nanoparticle volume fractions required for the onset of stabilization observed experimentally. When this was explicitly accounted for in their simulations, they made predictions that were in good agreement with the original experimental observations of Lewis and co-workers.[1,13,17] They also probed the effects of particle size ratio by varying the microsphere diameter at a fixed nanoparticle size. They reported

* Corresponding author. E-mail: jalewis@illinois.edu.

(1) Tohver, V.; Smay, J. E.; Braem, A.; Braun, P. V.; Lewis, J. A. *PNAS* **2001**, *98*, 8950–8954.
(2) Chan, A. T.; Lewis, J. A. *Langmuir* **2005**, *21*, 8576–8579.
(3) Lewis, J. A. *Adv. Mater.* **2006**, *16*, 2193–2204.
(4) Lee, A. Y.; Myerson, A. S. *MRS Bulletin* **2006**, *31*, 881–885.
(5) Rolland, A. *Pharmaceutical Particulate Carriers: Therapeutic Applications*; Marcel Dekker: New York, 1993.
(6) Shah, P. *MRS Bulletin* **2006**, *31*, 894–899.
(7) Shekunov, B. Y.; Chattopadhyay, P.; Tong, H. H. Y.; Chow, A. H. L. *Pharm. Res.* **2007**, *24*, 203–227.
(8) Braun, P. V.; Wiltzius, P. *Nature* **1999**, *402*, 603–604.
(9) Joannopoulos, J. D.; Villeneuve, P. R.; Fans, R. *Nature* **1997**, *386*, 143–149.
(10) Lee, W.; Pruzinsky, S. A.; Braun, P. V. *Adv. Mater.* **2002**, *14*, 271–274.
(11) Lee, W.; Chan, A.; Bevan, M. A.; Lewis, J. A.; Braun, P. V. *Langmuir* **2004**, *20*, 5262–5270.
(12) Taton, T. A.; Norris, D. J. *Nature* **2002**, *416*, 685–686.
(13) Tohver, V.; Chan, A.; Sakurada, O.; Lewis, J. A. *Langmuir* **2001**, *17*, 8414–8421.
(14) Karanikas, S.; Louis, A. A. *PRL* **2004**, *93*, 248303.
(15) Liu, J.; Luijten, E. *PRL* **2004**, *93*, 247802.
(16) Asakura, S.; Oosawa, F. *J. Polym. Sci.* **1958**, *33*, 183.
(17) Martinez, C. J.; Liu, J.; Rhodes, S. K.; Luijten, E.; Weeks, E. R.; Lewis, J. A. *Langmuir* **2005**, *21*, 9978–9989.

10.1021/la800422g CCC: $40.75
Published on Web 09/24/2008

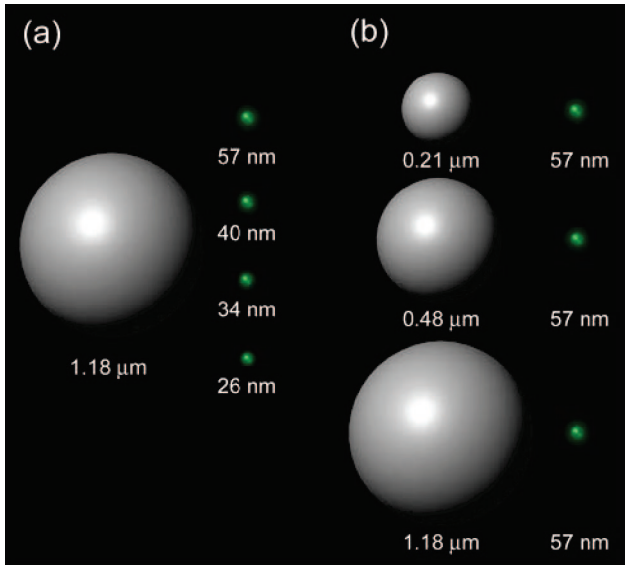

Figure 1. Schematic representation of an experimental system, in which the microsphere−nanoparticle size ratio is varied by either (a) changing the nanoparticle effective size at a fixed microsphere diameter through ionic strength variations or (b) changing the microsphere diameter at a fixed nanoparticle effective size.

that the window of stability was enhanced, as the microsphere−nanoparticle size ratio increased. However, neither the theoretical modeling nor the simulation efforts explicitly account for van der Waals attractions between microspheres, which both drive colloidal aggregation in the experimental systems of interest and lessen with decreasing microsphere size.

Here, we explore size ratio effects on the interparticle interactions and phase behavior of model binary mixtures composed of silica microspheres and highly charged polystyrene nanoparticles. Two approaches are pursued simultaneously (Figure 1). In the first approach, we fix the microsphere diameter while varying the effective nanoparticle diameter by adjusting the ionic strength of these mixtures. In the second approach, we fix the ionic strength and hence the effective nanoparticle diameter and vary the diameter of the microspheres in the mixtures. The experimental observations obtained in each approach are compared to the theoretical and simulation predictions described above. The first approach loosely mimics the work of Karanikas and Louis[14] yet avoids the experimental difficulties associated with simultaneously controlling both the nanoparticle size and surface charge, and the second approach is akin to the simulations carried out by Liu and Luijten.[15]

Experimental Section

Materials System. Monodisperse silica microspheres of varying size serve as the larger colloidal species. The largest microspheres (Geltech; Orlando, FL) have an average diameter of $1.18 \pm 0.02\ \mu$m and a density of 2.25 g/cm^3, as determined by helium pycnometry (model Accupyc 1330, Micrometrics Instruments Corp., Norcross, GA). The two smaller microspheres (Fiber Optic Center Inc., New Bedford, MA) have average diameters of 0.484 ± 0.016 and $0.212 \pm 0.016\ \mu$m, respectively, and a density of 1.97 g/cm^3. Their isoelectric point occurs at pH ∼2.5. They possess a zeta potential of −1 mV at pH 3 as determined by microelectrophoresis (ZetaSizer 3000, Malvern Instruments, Northborough, MA) on dilute suspensions ($\phi_{micro} = 1 \times 10^{-5}$) at a Debye screening length (κ^{-1}) of ∼9.6 nm.

Sulfate-functionalized polystyrene nanoparticles (IDC, Portland, OR), with an average diameter, σ_{nano}, of 19 ± 3 nm, serve as the smaller colloidal species in these mixtures. Their zeta potential is −120 mV at pH 3. Their density is 1.055 g/cm^3, and their refractive index is 1.591 at 590 nm.[18] Both pure and fluorescently labeled nanoparticles are used, with the latter having a peak excitation/emission wavelength of 475/520 nm.

Suspension Preparation. Binary mixtures are prepared by adding an appropriate volume fraction of the nanoparticles to deionized water preadjusted to pH 3 with nitric acid (reagent grade, Fisher Scientific). Sodium nitrite (reagent grade, Fisher Scientific) is added to adjust the ionic strength of solution. An appropriate amount of the silica stock suspension at pH 3 ($\phi_{micro} = 5 \times 10^{-4}$ to 3×10^{-1}) is then added, followed by ultrasonication (model 550 sonic dismembrator, Fisher Scientific, Pittsburgh, PA).

Fluorimetric Analysis of Nanoparticle Halo Formation. Binary mixtures ($\phi_{micro} = 1 \times 10^{-1}$) are prepared with either fluorescent nanoparticles ($\phi_{nano} = (0-1) \times 10^{-3}$) or a mixture of fluorescent and nonfluorescent nanoparticles, when $\phi_{nano} > 1 \times 10^{-3}$. The suspensions are capped to minimize solvent evaporation and are then kept in the dark during gravity-driven sedimentation. After microsphere sedimentation is complete, a 300 μL aliquot is taken from each supernatant solution for fluorescence intensity analysis. Solutions of known fluorescent nanoparticle concentration are used as a calibration standard. The fluorescence intensity measurements are carried out with a steady-state spectrofluorometer (model Quantamaster QM-4, Photon Technology International, Inc., Birmingham, NJ). The nanoparticles are excited at 475 nm, and the emission intensity is measured at 500−550 nm. The fluorescence intensity increases linearly with nanoparticle volume fraction, when $\phi_{nano} \leq 3 \times 10^{-3}$, beyond which the intensity reaches a plateau value. To overcome this limitation, mixtures of high nanoparticle volume fractions are prepared with a fixed concentration of fluorescent nanoparticles with a volume fraction of 1×10^{-3}, with the balance composed of their nonfluorescent (white) counterparts. The average peak intensities from 518 to 520 nm are used to determine number of nanoparticles associated with the microspheres in suspension.

The number of nanoparticles within the halo that surrounds each microsphere is calculated from the measured fluorescence intensity using

$$\frac{N_{nano}}{N_{micro}} = \frac{(I_{ini} - I_{final} - c)}{m\phi_{micro}}\left(\frac{\sigma_{micro}}{\sigma_{nano}}\right)^3 \qquad (1)$$

where I_{ini} and I_{final} are the expected and measured fluorescence intensities of nanoparticles in the supernatant and m and c are the slope and intercept, respectively, of the calibration curve obtained by measuring the fluorescence intensity of control solutions of known nanoparticle volume fraction.

Zeta Potential Analysis. The electrophoretic mobility of the microspheres in the binary mixtures is measured using a capillary flow cell of Zetasizer 3000HS at a constant applied field of 150 V. The suspensions contain $\phi_{micro} = 10^{-5}$ for $\sigma_{micro} = 1.18$ and 0.484 μm and $\phi_{micro} = 10^{-4}$ for $\sigma_{micro} = 0.212\ \mu$m and nanoparticle volume fractions that range from 0 to 10^{-4}. Note that the microsphere volume fraction for the smallest size ratio studied is increased by an order of magnitude because of their weak scattering intensity. To our knowledge, there is no simple theoretical model that accurately calculates the effective zeta potential from the electrophoretic mobility of weakly or dynamically interacting colloidal mixtures. We therefore relate the measured electrophoretic mobility of microspheres within these binary mixtures to an effective zeta potential (ζ_{eff}) based on the analysis by O'Brien and White.[19,20] We assume that the effective zeta potential contains contributions from both bare and nanoparticle-haloed regions around the microsphere surfaces. The measured zeta potential is related to the surface charge (Q) of a particle by the Loeb equation[20]

$$Q = \pi\varepsilon\varepsilon_0\frac{kT}{ze_0}\kappa\sigma^2\left\{2\sinh\left(\frac{ze\zeta}{2kT}\right) + \frac{8}{\kappa\sigma}\tanh\left(\frac{ze\zeta}{4kT}\right)\right\} \qquad (2)$$

where kT is the thermal energy, z is the charge of ions in solution, e is the electron charge, $\varepsilon\varepsilon_0$ is the dielectric constant of the solution, κ^{-1} is the Debye screening length, and σ is the particle diameter. From these data, we determine the total surface charge density by

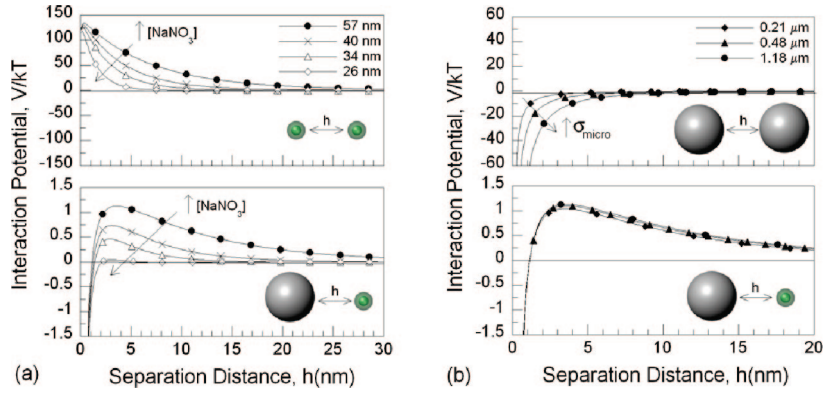

Figure 2. DLVO interparticle interaction potentials for microsphere−nanoparticle mixtures showing the effects of (a) varying the nanoparticle effective size at a fixed microsphere size of 1.18 μm and (b) varying the microsphere diameter at a fixed nanoparticle effective size of 57 nm.

summing the charge densities from the nanoparticles within each halo and from the bare microspheres, thus calculating the number of haloing nanoparticles per microsphere by

$$Q_{\text{eff}} = \left(\frac{N_{\text{nano}}}{N_{\text{micro}}}\right) Q_{\text{nano}} + Q_{\text{micro}} \tag{3}$$

where Q_{nano} and Q_{micro} are the surface charges of nanoparticles and bare microspheres, respectively. Note that under the experimental conditions of interest the bare microspheres are negligibly charged.

Bulk Sedimentation. Colloidal microspheres ($\phi_{\text{micro}} = 1 \times 10^{-1}$) suspended in the binary mixtures ($\phi_{\text{nano}} = 0 - 5 \times 10^{-2}$) undergo gravity-driven sedimentation in glass cylindrical cells (8 cm in height and 0.5 mm i.d.). Each sample cell is fabricated by attaching the glass cylinder tube to a no. 1 cover slide using polydimethylsiloxane (PDMS, Slygard 186, Dow Corning, Midland, MI). Both the cylinders and cover slides are cleaned with a 2.3:1 ratio of sulfuric acid (reagent grade, Fisher Scientific)/hydrogen peroxide (30% Fisher scientific) mixtures for 1 h and then repeatedly washed with deionized water and dried under nitrogen.

The binary suspensions are initially opaque; however, as the microspheres settle, the suspensions separate into a clear supernatant, a cloudy solution, and opaque sediment. This process is imaged using time-lapse photography with a video camcorder (Digital Handycam Camcorder, Sony, Japan) controlled by SupervisionCam Software (P. Krist, Herrsching, Germany). The initial microsphere sedimentation velocity (V) is determined by tracking the interface between the clear supernatant and cloudy regions. The microsphere sedimentation velocity (V_{micro}) at a given microsphere volume fraction is given by[21]

$$V_{\text{micro}} = V_0(1 - \phi_{\text{micro}})^n \tag{4}$$

where V_0 is the settling velocity for an isolated microsphere determined by Stokes' law

$$V_0 = \frac{2}{9}\frac{(\rho_{\text{micro}} - \rho)\sigma_{\text{micro}}^2 g}{4\eta} \tag{5}$$

where ρ_{micro} is the microsphere density, ρ is the density of the liquid phase, η is the apparent solution viscosity ($\eta = 1$ mPa·s for water), g is the gravitational constant, and n is a power law exponent (= 6.55). The microsphere sedimentation velocity, V_{micro}, is found to be 1.5×10^{-5}, 7.6×10^{-5}, and 5.8×10^{-4} mm/s in stable suspensions ($\phi_{\text{micro}} = 0.1$) with microsphere diameters of 0.212, 0.484, and 1.18 μm, respectively. The microsphere sediment volume fraction (ϕ_{sediment}) is determined by measuring the final sediment height after several weeks.

Direct Imaging of Binary Mixtures. Confocal laser scanning microscopy is used to directly image the structure of colloidal phases assembled under gravity from binary mixtures of varying composition and size ratio. The samples are imaged both during assembly and after 3 weeks of sedimentation by placing them on an inverted optical microscope (Leica SP2) equipped with Ar and He/Ne laser sources providing both 488 and 633 nm laser lines and a 63×/1.4 NA oil lens. Images are acquired simultaneously by two photomultiplier tubes (PMTs); one is used to acquire reflected light from both microspheres and nanoparticles (613 to 653 nm), and the other is used to detect light emitted from fluorescent nanoparticles (500 and 540 nm). The samples are scanned in both the $x-y$ and $x-z$ directions (i.e., parallel and perpendicular to the glass substrate, respectively). The sedimented samples are essentially static and do not evolve during this time. Multiple volumetric regions are scanned per sample with each volume containing between ~500 and 4000 particles depending on whether sedimentation initially occurs from the gel or the stable fluid phase.

Results and Discussion

Size Ratio Effects on Interparticle Interactions. The microsphere−microsphere, nanoparticle−nanoparticle, and microsphere−nanoparticle interaction potentials for our binary mixtures are shown in Figure 2. These potentials are calculated using Derjaguin−Landau−Verwey−Overbeek (DLVO) theory[22,23] in which the van der Waals (vdW) potential[4,22,23] is determined by Lifshitz theory[24] and the electrostatic interactions are calculated using the linear superposition approximation (LSA)[22,25−27] (Supporting Information). The microspheres are negligibly charged, hence vdW interactions dominate, leading to a net attraction between these species that intensifies with increasing microsphere diameter. The depth of this attractive minimum, defined at an arbitrary cutoff distance of $h = 1$ nm, is approximately $-11kT$, $-30kT$, and $-60kT$ for $\sigma_{\text{micro}} = 0.21$, 0.48, and 1.18 μm, respectively. By contrast, the highly charged nanoparticles exhibit a strong electrostatic repulsion leading to

(18) *CRC Handbook of Chemistry and Physics*; 71 ed.; CRC Press: Boca Raton.
(19) O'Brien, R. W.; White, L. R. *J. Chem. Soc. Faraday Trans.* **1978**, *74*, 1607–1626.
(20) Hunter, R. J. *Zeta Potential in Colloid Science: Principles and Applications*; Academic Press Inc.: New York, 1981.
(21) Russel, W. B., Saville, D. A., and Schowalter, W. R., *Colloidal Dispersions*; Cambridge University Press: Cambridge, 1989.
(22) Hunter, R. J. *Foundations of Colloid Science*; Oxford University Press: New York, 1995; Vol. *I.*
(23) Israelachvili, J. *Intermolecular and Surf. Forces*; 2 ed.; Academic Press: San Diego, 1992.
(24) Prieve, D. C.; Russel, W. B. *J. Colloid Interface Sci.* **1988**, *125*, 1–13.
(25) Bell, G. M.; Levine, S.; McCartney, L. N. *J. Colloid Interface Sci.* **1970**, *33*, 335–359.
(26) Warszynski, P.; Adamczyk, Z. *J. Colloid Interface Sci.* **1997**, *187*, 283–295.
(27) Ohshima, H.; Healy, T. W.; White, L. R. *J. of Chem. Soc., Faraday Trans. 2* **1983**, *79*, 1613–1628.

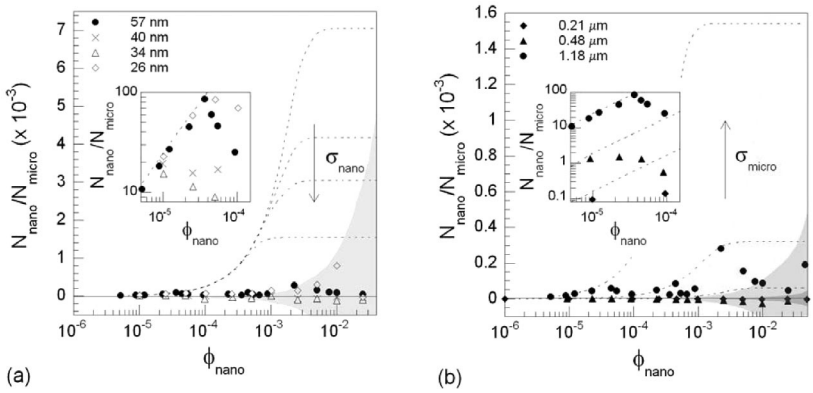

Figure 3. Nanoparticle halo formation in binary mixtures of varying size ratio, where (a) the nanoparticle effective size is varied at a fixed microsphere diameter of 1.18 μm by changing the ionic strength and (b) the microsphere diameter is varied at a fixed nanoparticle effective size of 57 nm. The shaded gray areas represent measurement errors, which become darker with decreasing size ratios. Dashed lines represent the predicted monolayer coverage for each binary mixture, and arrows denote the direction of increasing particle size. The insets highlight the extent of nanoparticle halo formation at the lowest nanoparticle volume fractions studied for each system.

Table 1. Nanoparticle Size Effects on Halo Formation[a]

	fluorometric analysis			zeta potential analysis		
σ_{nano}^{eff} (nm)	N_{nano}/N_{micro}	ϕ_{halo}^{eff}	L_{halo} (nm)	N_{nano}/N_{micro}	ϕ_{halo}^{eff}	L_{halo} (nm)
57	50	0.028	300	136	0.050	225
40	0	0		205	0.039	178
34	0	0		286	0.037	157
26	350	0.043	112	363	0.029	136

[a] Microsphere diameter = 1.18 μm.

Table 2. Microsphere Size Effects on Halo Formation[a]

	fluorometric analysis			zeta potential analysis		
$\sigma_{micro}/\sigma_{nano}^{eff}$	N_{nano}/N_{micro}	ϕ_{halo}^{eff}	L_{halo} (nm)	N_{nano}/N_{micro}	ϕ_{halo}^{eff}	L_{halo} (nm)
21	50	0.028	300	136	0.050	225
8	1.5	0.006	658	40	0.139	135
4	0	0		7	0.127	142

[a] Effective nanoparticle diameter = 57 nm.

an effective size that increases with decreasing ionic strength, where $\sigma_{nano}^{eff} = \sigma_{nano} + \lambda$ and λ is defined by the minimum separation distance at which their repulsion first exceeds kT. On the basis of these calculations, we find that the nanoparticle effective diameters are 57, 40, 34, and 26 nm for κ^{-1} values of 9.6, 5.1, 3.3, and 1.7 nm, respectively. Finally, the microsphere−nanoparticle interactions exhibit a weak repulsion ($\sim kT$) that precedes a modest attractive well ($\sim$several kT in magnitude) in these binary mixtures. This weak repulsive barrier decreases considerably with increasing ionic strength until it completely disappears when $\kappa^{-1} = 1.7$ nm. Interestingly, the microsphere−nanoparticle interaction potentials exhibit little variation as the microsphere size is varied from 0.21 to 1.18 μm at a fixed effective nanoparticle diameter of 57 nm, which corresponds to a ratio of microsphere diameter to effective nanoparticle size that ranges from 4 to 21, respectively.

Nanoparticle Halo Formation. The extent of nanoparticle halo formation observed in binary mixtures of varying size ratio is shown in Figure 3. In each case, the number of nanoparticles that reside near the microsphere surfaces is far below the monolayer coverage reported for strongly attractive systems.[2] However, as the insets reveal, a modest number of nanoparticles associate with each microsphere, N_{nano}/N_{micro}, in these weakly interacting systems (Table 1). Because the nanoparticle concentration in solution becomes significantly enhanced with increasing nanoparticle volume fraction, there is pronounced scatter in the measurements under these conditions. The observed error is ±5% of the measured fluorescence intensity, as denoted by the shaded gray area in each plot. As the nanoparticle effective size decreases, there is a slight increase in the extent of nanoparticle haloing. Barr and Luijten[27] reported that a microsphere−nanoparticle attraction ranging from $-5kT$ to $-10kT$ at $h = 0.4$ nm is sufficient to induce the modest haloing observed experimentally for mixtures of the largest size ratio. As the microsphere size decreases, the total surface area per microsphere in suspension is reduced, hence fewer nanoparticles per microsphere are required to achieve a similar effective coverage, $\phi_{halo}^{eff} \sim N_{nano}/4N_{micro}(\sigma_{nano}^{eff}/\sigma_{micro})^2$, for a given nanoparticle effective size (Figure 3b and Table 2). Note that the N_{nano}/N_{micro} values reported in Tables 1 and 2 are determined by averaging the data measured beyond the initial sharp rise in halo formation observed in the insets shown in Figure 3.

To probe the extent of nanoparticle halo formation further, we measure the microsphere effective zeta potential in binary mixtures of varying size ratio. These data are shown in Figure 4. In all binary mixtures studied, the magnitude of the microsphere effective zeta potential, ζ_{eff}, increases with increasing nanoparticle volume fraction. The number of nanoparticles that form halos around each microsphere, N_{nano}/N_{micro}, is calculated from the maximum microsphere effective zeta potentials using eqs 2 and 3 and reported in Tables 1 and 2. As the effective nanoparticle size decreases, there is a 2-fold increase in the maximum value of effective microsphere zeta potential, indicative of enhanced nanoparticle haloing that increases from $N_{nano}/N_{micro} \approx 130-360$ over the experimental conditions probed. Even though the number ratio increases, the effective nanoparticle volume fraction within the halo that surrounds each microsphere, ϕ_{halo}^{eff}, is actually reduced from 0.050 to 0.029 as the effective nanoparticle diameter decreases from 57 to 26 nm at a fixed microsphere diameter of 1.18 μm. By contrast, the maximum values of effective microsphere zeta potential exhibit little variation over a 6-fold increase in the microsphere size. Notably, the number of nanoparticles per microsphere required to achieve the same microsphere effective zeta potential of −20 mV decreases from $\sim$ 130 to 10 with decreasing microsphere size. Nevertheless, this leads to a concurrent increase in the effective nanoparticle volume fraction within these halos (i.e., ϕ_{halo}^{eff} ranges from 0.050 to 0.127) as the microsphere diameter decreases from 1.18 to 0.212 μm at a fixed effective nanoparticle diameter of 57 nm. In all mixtures studied, the nanoparticle halos that surround each microsphere are dilute in nature (i.e., the lateral separation distance between

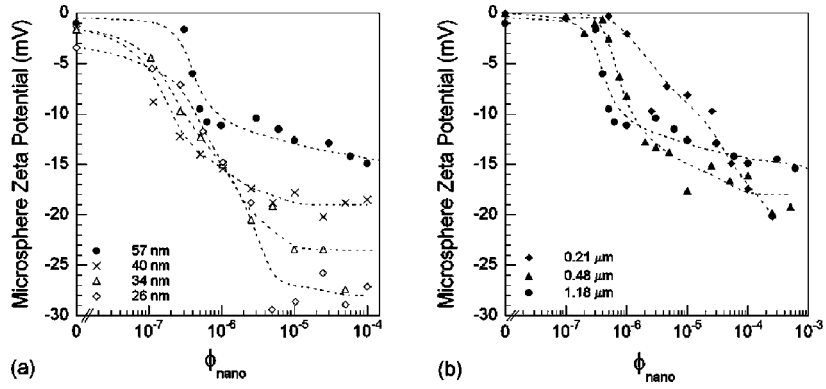

Figure 4. Effective zeta potential of microspheres in binary mixtures of varying size ratio, where (a) the nanoparticle effective size is varied at a fixed microsphere diameter of 1.18 μm by changing the ionic strength and (b) the microsphere diameter is varied at a fixed effective nanoparticle size of 57 nm. (Dashed lines merely serve to guide the eye).

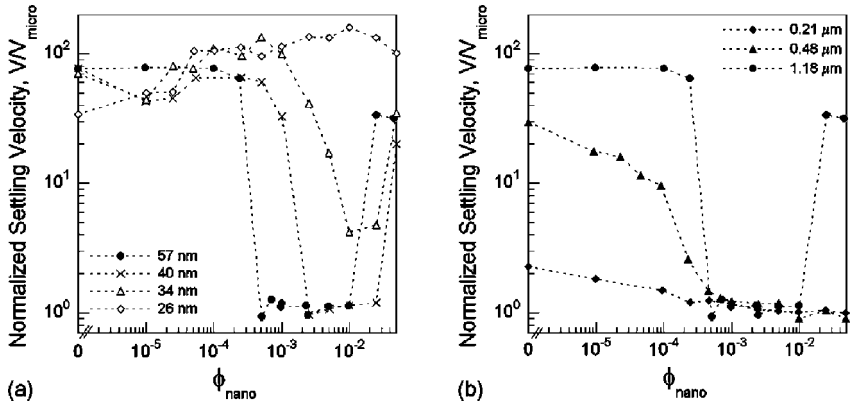

Figure 5. Normalized settling velocity of microspheres in binary mixtures of varying size ratio, where (a) the nanoparticle effective size is varied at a fixed microsphere diameter of 1.18 μm by changing ionic strength and (b) the microsphere diameter is varied at a fixed effective nanoparticle size of 57 nm. (Dashed lines merely serve to guide the eye).

nanoparticles, $L_{halo} = (\pi(\sigma_{nano}^{eff})^2/4\phi_{halo}^{eff})^{1/2}$ significantly exceeds their effective size (Tables 1 and 2).

Size Ratio Effects on Colloidal Stability. The effects of the particle size ratio on the phase behavior of binary mixures are investigated through a combination of bulk sedimentation measurements and confocal imaging of the assembled colloidal phases. The normalized microsphere sedimentation velocity is plotted as a function of nanoparticle volume fraction for representative mixtures of fixed $\phi_{micro} = 0.1$, in which either the nanoparticle effective size or microsphere size is varied (Figure 5). These data are normalized by V_{micro}, the sedimentation velocity of an individual microsphere, to allow direct comparison between each system. In the absence of nanoparticles, negligibly charged microspheres undergo rapid flocculation and sedimentation, yielding an open sediment ($\phi_{sediment} \approx 0.2-0.3$). For binary mixtures of varying effective nanoparticle diameter, shown in Figure 5a, the microspheres become stabilized upon the addition of a lower critical nanoparticle volume fraction and settle individually ($V/V_{micro} \approx 1$) to yield a dense sediment ($\phi_{sediment} = 0.55$) at low ionic strength (i.e., for mixtures that contain nanoparticles of effective size, σ_{nano}^{eff} of 40 and 57 nm). In these mixtures, microsphere stability is reversed upon the addition of an upper critical nanoparticle volume fraction. At an intermediate ionic strength (i.e., for mixtures that contain nanoparticles of effective size, σ_{nano}^{eff} of 34 nm), the microspheres become only slightly stabilized upon the addition of a lower critical nanoparticle volume fraction, as evidenced by the fact that the normalized sedimentation velocity of microspheres exceeds unity. Interestingly, at even higher ionic strength (i.e., for mixtures that contain nanoparticles of effective size, σ_{nano}^{eff}, of 26 nm), the microspheres remain flocculated and settle rapidly over the entire range of nanoparticle volume fractions explored. This occurs even though the effective microsphere zeta potential is highest in this system (Figure 4a). We speculate that the reduced enrichment of nanoparticles in the halo, ϕ_{halo}^{eff}, relative to the bulk solution under such conditions renders the mixtures unstable over the entire range of nanoparticle concentrations explored. Thus, the width of the stability window, $\phi_{nano}^{U,C}/\phi_{nano}^{L,C}$, decreases from 50 to 20 to 8 to 0 with decreasing effective nanoparticle size. It is noteworthy that when the data in Figure 5a are plotted as a function of effective nanoparticle volume fraction, ϕ_{nano}^{eff}, the onset of stability and reentrant gelation as defined by $\phi_{nano}^{L,C}$ and $\phi_{nano}^{U,C}$ respectively, each occurs at nearly identical values of $\phi_{nano}^{eff} \approx 0.01$ and 0.4, respectively, in bulk solution (Supporting Information).

Negligibly charged microspheres of varying size undergo flocculation and sedimentation at normalized velocities that decrease with decreasing size, σ_{micro}, in the absence of nanoparticles (Figure 5b). The observed differences in their sedimentation behavior reflect the diminished vdW attraction between microspheres as the microsphere size decreases, which gives rise to a reduction in their characteristic cluster size from 13 to 3 to 0.5 μm for microspheres with diameters of 1.18, 0.48, and 0.21 μm, respectively. In binary mixtures of varying microsphere size, the microspheres become stabilized upon the addition of a lower critical nanoparticle volume fraction of $\sim 5 \times 10^{-4}$ and settle individually ($V/V_{micro} \approx 1$) to yield a dense sediment ($\phi_{sediment} = 0.55$). The uniform value of the nanoparticle volume fraction required for stabilization reveals that stabilization again occurs

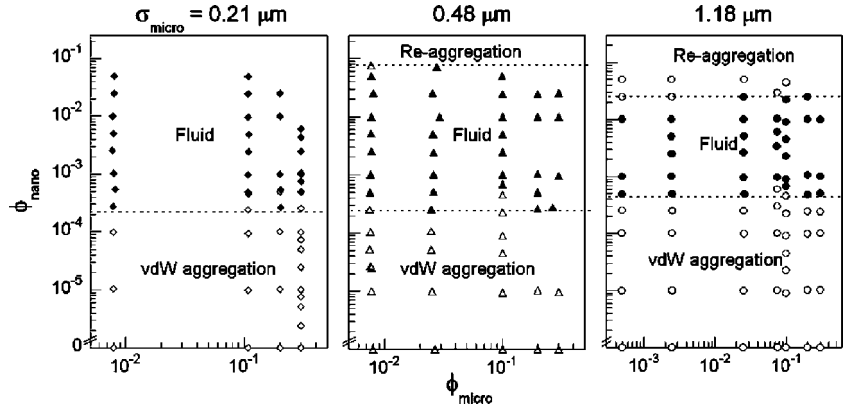

Figure 6. Phase diagrams for binary mixtures of varying microsphere diameter at a fixed nanoparticle effective size of 57 nm, showing unstable (open symbol) and stable (filled symbol) regions.

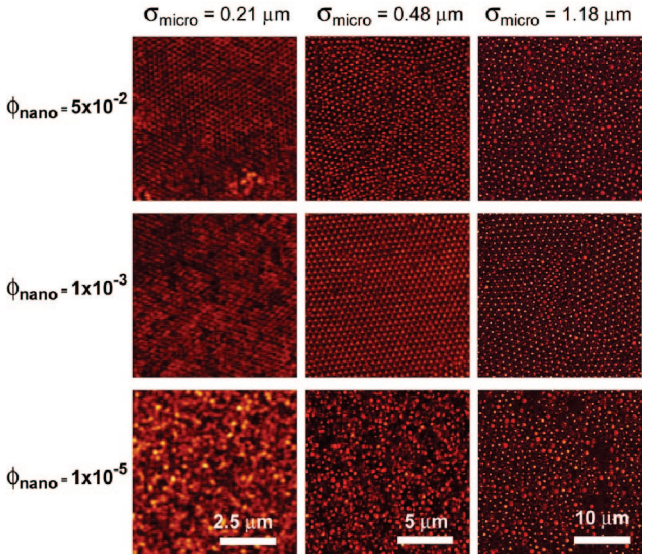

Figure 7. Confocal images ($x-y$ scans) of sediments assembled from binary mixtures of varying microsphere size.

at nearly identical values of a nanoparticle effective volume fraction of ~0.01 for these mixtures over the range of microsphere sizes studied. By contrast, the bulk sedimentation measurements show that the onset of reentrant gelation is strongly dependent on the particle size ratio. A sharp rise in normalized settling velocity, indicative of microsphere flocculation, is observed only for binary mixtures composed of the largest microspheres.

To explore their stability further, we produced the phase diagrams shown in Figure 6 for binary mixtures of varying composition and microsphere diameter. Interestingly, $\phi_{nano}^{L,C}$ is nearly identical for all three mixtures independent of their size ratio, where $\phi_{nano}^{L,C} \approx (2-4) \times 10^{-4}$. When $\phi_{nano} < \phi_{nano}^{L,C}$, the microspheres flocculate because of vdW forces and form an open gel upon sedimentation. When $\phi_{nano}^{L,C} \delta\ \phi_{nano} \leq \phi_{nano}^{U,C}$, the microspheres are fully stabilized, yielding a fluid phase from which an opalescent crystalline sediment forms (Figure 7). Finally, when $\phi_{nano} \geq \phi_{nano}^{U,C}$, the microspheres undergo reentrant gelation because of a depletion attraction that deviates from the standard A−O behavior.[16] The value of $\phi_{nano}^{U,C}$ is expected to increase with decreasing size ratio but, in fact, is not clearly observed for binary mixtures with the smallest effective size ratios of 4−8. Unfortunately, we are unable to prepare mixtures at higher nanoparticle volume fraction than those reported in Figures 6 and 7 because nanoparticle flocculation occurs when $\phi_{nano} > 0.05$. Nevertheless, similar to standard depletion studies, we expect that microsphere reaggregation should be greatly suppressed as the size ratio nears unity.

Several important observations emerge from our investigation of particle size ratio effects on the behavior of binary mixtures of high charge asymmetry. First, we find that the onset of stabilization occurs at the same effective nanoparticle volume fraction in bulk solution, $\phi_{nano}^{eff} \approx 0.01$, independent of the nanoparticle effective size or microsphere−nanoparticle size ratio, except for mixtures with the highest ionic strength in which stabilization is not observed. Importantly, for systems that undergo stabilization, we find that there is a pronounced enrichment of nanoparticles near the microsphere surfaces relative to the bulk solution. On average, a nearly 10-fold enhancement, where an effective nanoparticle halo volume fraction of $\phi_{halo}^{eff} \approx 0.07$, is calculated for such mixtures on the basis of the effective microsphere zeta potential measurements (Tables 1 and 2). Second, our observations support the findings of Luijten and co-workers[15,28] that a weak attraction (~several kT) between microsphere−nanoparticle species is necessary to induce the formation of nanoparticle halos at the low absolute values of nanoparticle volume fraction observed experimentally. Finally, both Karanikas and Louis[14] and Liu and Luijten[15] predicted that the window of stability, defined as $\phi_{nano}^{U,C}/\phi_{nano}^{L,C}$, increased with increasing nanoparticle effective diameter and microsphere−nanoparticle size ratio. Although our observations are in good agreement with the former prediction, we find that the opposite is true as the microsphere−nanoparticle effective size ratio increases. This discrepancy may arise because neither of these approaches explicitly considers the effects of van der Waals interactions between microspheres that both drive colloidal aggregation in the experimental system of interest and lessen with decreasing microsphere size. Quite recently, Scheer and Schweizer developed a more comprehensive theoretical framework for microsphere−nanoparticle mixtures of high charge and size asymmetry.[29] They found that the interactions between microspheres in the presence of highly charged nanoparticles not only grew more strongly with nanoparticle volume fraction but did so in a complex, potential-specific manner when the underlying van der Waals attraction between such species was taken into consideration. Clearly, further experimental, simulation, and modeling efforts are warranted to fully elucidate the rich behavior observed in these binary systems.

(28) Barr, S. A.; Luijten, E. *Langmuir* **2006**, *22*, 7152–55.
(29) Scheer, E. N.; Schweizer, K. S. *J. Chem. Phys.* **2008**, *128*, 164905.

Conclusions

We have studied the interparticle interactions and phase behavior of microsphere−nanoparticle mixtures of high charge asymmetry and varying size ratio. Binary mixtures, in which the effective nanoparticle diameter is reduced at a fixed microsphere diameter, exhibit a narrower window of stability that ultimately disappears with increasing ionic strength. By contrast, binary mixtures of varying microsphere diameter and fixed effective nanoparticle size are stabilized at similar nanoparticle volume fractions and exhibit a broader window of stability with decreasing effective size ratio. Surprisingly, nanoparticle haloing promotes colloidal stability even in mixtures in which the effective size ratio approaches unity. This unexpected observation may arise from the reduced attraction between microspheres as their size decreases. Our observations further showcase the rich complexity that governs the behavior of microsphere−nanoparticle mixtures of high charge and size asymmetry and point to the growing practical importance of this novel route for tuning suspension stability.

Acknowledgment. This material is based on work supported by the U.S. Department of Energy, Division of Materials Science, under award nos. DEFG02-01ER45941 and DEFG02-07ER46471. We gratefully acknowledge K. Schweizer, E. Luijten, C. Martinez, and J. Gilchrist for useful discussions. A.T.C. was partially supported by an NSF Graduate Research Fellowship.

Supporting Information Available: Modeling of interparticle interactions. This material is available free of charge via the Internet at http://pubs.acs.org.

LA800422G